Since January 2020 Elsevier has created a COVID-19 resource centre with free information in English and Mandarin on the novel coronavirus COVID-19. The COVID-19 resource centre is hosted on Elsevier Connect, the company's public news and information website.

Journal of Thermal Biology 112 (2023) 103444

Contents lists available at ScienceDirect

Journal of Thermal Biology

journal homepage: www.elsevier.com/locate/jtherbio

Infrared image method for possible COVID-19 detection through febrile and subfebrile people screening☆

Marcos Leal Brioschi [a], Carlos Dalmaso Neto [a,b,*], Marcos de Toledo [a], Eduardo Borba Neves [c], José Viriato Coelho Vargas [b], Manoel Jacobsen Teixeira [d]

[a] Medical Thermology and Thermography Specialization, Hospital das Clínicas da Faculdade de Medicina da Universidade de São Paulo, HCFMUSP, São Paulo, SP, 01246-903, Brazil
[b] Mechanical Engineering Post-Graduation Program, Mechanical Engineering Department, Universidade Federal do Paraná, UFPR, Curitiba, PR, 81531-980, Brazil
[c] Biomedical Engineering Post-Graduation Program, Universidade Tecnológica Federal do Paraná, UTFPR, Curitiba, PR, 82590-300, Brazil
[d] Neurology and Neurosurgery Department, Hospital das Clínicas da Faculdade de Medicina da Universidade de São Paulo – HCFMUSP, São Paulo, SP, 01246-903, Brazil

ARTICLE INFO

Keywords:
Infrared imaging
Artificial intelligence
Convolutional neural network

ABSTRACT

This study proposed an infrared image-based method for febrile and subfebrile people screening to comply with the society need for alternative, quick response, and effective methods for COVID-19 contagious people screening. The methodology consisted of: (i) Developing a method based on facial infrared imaging for possible COVID-19 early detection in people with and without fever (subfebrile state); (ii) Using 1206 emergency room (ER) patients to develop an algorithm for general application of the method, and (iii) Testing the method and algorithm effectiveness in 2558 cases (RT-qPCR tested for COVID-19) from 227,261 workers evaluations in five different countries. Artificial intelligence was used through a convolutional neural network (CNN) to develop the algorithm that took facial infrared images as input and classified the tested individuals in three groups: fever (high risk), subfebrile (medium risk), and no fever (low risk). The results showed that suspicious and confirmed COVID-19 (+) cases characterized by temperatures below the 37.5 °C fever threshold were identified. Also, average forehead and eye temperatures greater than 37.5 °C were not enough to detect fever similarly to the proposed CNN algorithm. Most RT-qPCR confirmed COVID-19 (+) cases found in the 2558 cases sample (17 cases/89.5%) belonged to the CNN selected subfebrile group. The COVID-19 (+) main risk factor was to be in the subfebrile group, in comparison to age, diabetes, high blood pressure, smoking and others. In sum, the proposed method was shown to be a potentially important new tool for COVID-19 (+) people screening for air travel and public places in general.

1. Introduction

Fever is one of the most important clinical signs for infection recognition (Chiappini et al., 2011; Liu et al., 2004; Ng, 2012; Shi et al., 2020; Teran et al., 2012). Thermal infrared method detection for fever screening, image associated or not, is currently in use worldwide to control people for air travel and access to public places, aiming at COVID-19 spread containment (Chiappini et al., 2011; Chiu et al., 2005; Ghassemi et al., 2018; Goeijenbier et al., 2014; Huang et al., 2020; Liu et al., 2004; Ng, 2012; Ng and Acharya, 2009; Ng and Kee, 2008; Nishiura and Kamiya, 2011; Shi et al., 2020; Teran et al., 2012; Yang et al., 2020).

Although questionable, the use of infrared has become popular because it is a highly sensitive and noninvasive method (Martinez-Jimenez et al., 2021; Ng et al., 2006; Nguyen et al., 2010; Nishiura and Kamiya, 2011; Ring and Ng, 2012) and high precision non-contact infrared thermometers are simple to operate. Infrared thermometers are innocuous and contagious risk-free by not having direct contact with the measuring instrument and are thus, appropriate for handling crowds in places with heavy human traffic. However, their accuracy and effectiveness in controlling the pandemic effects have been questioned (International Electrotechnical Commission & International Organization for Standardization, 2017; International Organization for

☆ The corresponding author attests that all listed authors meet authorship criteria and that no others meeting the criteria have been omitted.

* Corresponding author. Medical Thermology and Thermography Specialization, Hospital das Clínicas da Faculdade de Medicina da Universidade de São Paulo, HCFMUSP, São Paulo, SP, 01246-903, Brazil.
E-mail address: abraterm@abraterm.com.br (C. Dalmaso Neto).

https://doi.org/10.1016/j.jtherbio.2022.103444
Received 14 December 2021; Received in revised form 30 November 2022; Accepted 22 December 2022
Available online 28 December 2022

Nomenclature

CDC	Center of Diseases Control
CNN	convolutional neural network
DNN	deep neural network
ICA	image classification algorithm
h0	null hypothesis
N	number of people
NIST	National Institute of Standards and Technology
p	probability
ReLU	rectified linear unit
ROI	region of interest
Rt-qPCR	quantitative reverse transcription PCR
SaO_2	oxygen saturation, %
SP	Science Partner
T	temperature, °C
v	velocity, m s^{-1}

Greek letters

ε	emissivity
φ	relative humidity, %

Subscripts

air	air
avg	average
eye	eye
f	fever
fh	forehead
fth	fever threshold
ic	inner canthus area
ip	image pixel
max	maximum
ti	tested individuals
tot	total
ty	tympanic
∞	ambient

Superscript

$-$	mean value

Standardization, 2017; Mouchtouri et al., 2019; Ng and Chong, 2006). As a result, the United States Food and Drug Administration (FDA) established guidelines for COVID-19 control infrared imaging thermography (IT) correct use (International Electrotechnical Commission & International Organization for Standardization, 2017; International Organization for Standardization, 2017; U.S. Department of Health and Human Services et al., 2020).

Several aspects of the method are still debatable, and no consensus has been achieved to date. Not only is the most appropriate temperature recording site under discussion, i.e., forehead (Antabak et al., 2016; Chan et al., 2006; Chiang et al., 2008; Chiu et al., 2005; Hewlett et al., 2011; Ng et al., 2004, 2005; Sun et al., 2017), tympanic (Bernardo et al., 1999), eyes (Fitriyah et al., 2017; Mercer and Ring, 2003; Vardasca et al., 2019), temporal (Center for Disease Control and Prevention, 2020a; Cruz-Albarran et al., 2020; Teran et al., 2012; Zhou et al., 2020), but also the effect of the surroundings on the measurement accuracy (Dagdanpurev et al., 2018; Zhou et al., 2020), as well as the ceiling normal temperature for the general population fever tracking (Biomedical and Health Standards Committee, 2020a, 2020b; Childs, 2018; Gomolin et al., 2005; Zhou et al., 2020). Furthermore, the method might be proven ineffective in controlling COVID-19 spread caused by the coronavirus SARS-CoV-2, since it has been found that more than 70% of the people who contracted the virus do not even present fever in the initial stages of the disease (Bhat et al., 2020; Li et al., 2020; Michelen et al., 2020; Ng and Kaw, n. d.; Zhou et al., 2020).

Recently, humanity faced the so called severe acute respiratory syndrome (SARS), which is a respiratory contagious illness and sometimes lethal. For SARS, the number of cases that were identified due to fever detection was very low, thus major investments to allow for population fever screening were not justifiable (Ng, 2004). Another difficult hurdle was the impracticability of individually evaluating people in congested places (e.g., airports, stadiums) (Bitar et al., 2009; Cheung et al., 2012; Hay et al., 2004; Selent et al., 2013). The alternative of health-oriented forms to be filled out by travelers was also found ineffective for viral spread containment (Quilty et al., 2020).

Regarding the swine flu, caused by the H1N1 influenza virus, which is a nose, throat, and lungs infection, Brioschi et al. analyzed several febrile patients' facial thermal distribution. The study showed that facial infrared imaging had better potential than a fever indication temperature point value for early contagious people identification (Brioschi et al., 2010). A plausible physical explanation for such finding relies upon viral pathogenesis that occurs in various stages: (i) virus host exposure and system entry, (ii) host internal propagation, (iii) host response to the virus external stimulus (tropism), (iv) virus degree of pathogenicity (virulence), (v) viral infection and disease patterns, (vi) host factors, and (vii) host defense. More specifically, in stage (v) inflammatory abnormalities are triggered, the immune system is activated, generating systemic vasodilation and vasoconstriction in extremities before the patient develops clinical fever (Arons et al., 2020; Atkins and Bodel, 1972; Bai et al., 2020; Biomedical and Health Standards Committee, 2020b; Blatteis, 2007; Brioschi et al., 2010; Conti, 2004; Gowen et al., 2010; Michelen et al., 2020; Ng, 2004; Ng and Kaw, n. d.; Quilty et al., 2020; Saper, 1998). Hence, facial abnormal vasomotor behavior could be identified as an early sign of viral infection before the individual fever development.

1.1. Objective of the paper

Based on the bibliographic review and the questionable effectiveness of fever indication temperature point value for early COVID-19 contagious people identification, the general objective of this work was to propose an infrared image method for febrile and subfebrile COVID-19 patients screening. To achieve the general objective, the following specific objectives were devised: (i) Elaborate a methodology for utilizing facial infrared imaging as a noninvasive screening exam for possible COVID-19 early detection in people with and without fever (subfebrile state); (ii) Conceive and implement a computational algorithm for general application of the method considering multiple facial temperature points measurements, based on the analysis of a large number of selected emergency room patients, and (iii) Test the developed method and algorithm effectiveness for COVID-19 early detection in a large number of individuals of the general population in five different countries.

2. Materials and methods

2.1. Study design and participants

A convolutional neural network (CNN) was selected as the method to conduct the COVID-19 early detection in people with and without fever (subfebrile state) using facial infrared imaging. The method consists of a deep neural network (DNN), which is usually applied to visual imagery analyses. Convolutional neural networks are recognized as a remarkable tool in pattern recognition (NG et al., 2005; Valueva et al., 2020).

The DNN includes multiple layers between the input and output layers. The components are neurons, synapses, weights, biases, and functions, which operate similarly to the human mind, forming multilayer algorithms that could be trained.

The basic concept is that the DNN should be trained to recognize different patterns in a particular image and determine the probability that the image belongs to one of the patterns. An example would be the recognition of cattle breeds from cattle images, in which the DNN calculates the probability of an animal in the image to belong to a specific breed. In the current study, CNN was applied to select people with and without fever (subfebrile state) using facial infrared imaging. Then, the results were reviewed and the probabilities the network displayed (within pre-established limits) were selected, and the label was returned. A layer is defined by each mathematical manipulation, so that complex DNN depict many layers, namely deep networks.

The study was designed in two phases so that the CNN algorithm could be executed. In phase 1, a substantial sample of people allowed for building a standard facial infrared images data bank in two folders: no fever (1) and fever (2) cases. Phase 2 consisted of using the same artificial intelligence algorithm to analyze the facial images of a much larger number of individuals than in phase 1, for comparing to the standard data bank, and for creating a new algorithm that classified the cases in fever (1), intermediate or subfebrile (2), and no fever (3). Alternatively, such classification could be interpreted as high (1), medium (2), and low (3) risk to be a COVID-19 bearer, respectively.

2.2. Infrared camera calibration and precision assessment

Regarding camera calibration, the detector consisted of a focal plane array, uncooled microbolometer 320 × 240 pixels with a thermal sensitivity of 0.08 °C at 30 °C, spectral range of 7.5–13 μm, and measurement accuracy at ±1% of the real-time reading. The focal length from subject to scanner was 1 m.

All equipment were carefully calibrated by utilizing a blackbody source with an expanded uncertainty less than 0.1 °C (level of confidence of approximately 95%) before data collection, so that a good reading reproducibility capability could be achieved. Calibration was limited specifically to the human face. For that, the screening thermograph required that the operator framed the facial image in the workable target plane.

The thermal imager was tested against multiple high-end black bodies sources whose radiance temperature was calibrated with an expanded uncertainty not greater than 0.1 °C (level of confidence of approximately 95%), and stability better than ±0.002 °C. The calibrations were performed by a calibration laboratory competent in radiation thermometric calibrations, traceable to international measurement standard. For that, the service centers were certified according to ISO 9001, and temperature reference standards were traceable to the SP Technical Research Institute of Sweden, or the National Institute of Standards and Technology (NIST). The calibration of the camera was carried out using radiation sources that were traceable to National Standards at RISE, Research Institutes of Sweden and to NIST, National Institute of Standards and Technology (USA). The blackbody source had a radiance temperature range and control interval sufficient for the laboratory testing in accordance with this standard. The blackbody source had a known emissivity greater than 0.995. The diameter of the blackbody source aperture was sufficiently large so that the thermal imager's temperature measurement was not affected by it and to allow a clear identification of colour change at the workable plane.

In sum, the cameras used in this study were engineered and calibrated with automatic ambient drift compensation that eliminated the need for a black body reference all the time. Reasons for this include: i) Camera calibration was part of the production process and was based on multiple high-end black bodies sources; ii) The cameras integrated internal temperature sensors that compensated for possible calibration shifts; iii) A shutter between the camera detector and the lens was used as a reference to perform non-uniformity corrections when the camera environment changed; iv) Such proprietary mix of technologies ensured the thermal camera measurements remained stable and constant meeting the standard set forth in IEC 80601-2-59:2017, which states thermal cameras "may use *self-corrections* to maintain the drift within acceptable limits … to allow for substitution of the *calibration source*".

The permissible drift of a screening thermograph (i.e., infrared camera system) is less than or equal to 0.2 °C, over an interval of 14 days. Therefore, the herein utilized screening thermograph used self-corrections to maintain the drift within acceptable limits. Note also that thermography is understood as a tracking measurement, thus the focus from the epidemiologic point of view was to separate as many suspicious cases as possible, although several false positive cases could appear.

2.3. Standard data bank construction (phase 1)

Thermal images of the anterior face occupying 75% of the visual framework were obtained with an infrared thermal imager (320 × 240 pixels, T530sc, FLIR, TermoCam, Brazil; with a selected emissivity, $\varepsilon = 0.98$) with the standing individual looking directly at the sensor lens with a 90° angle, at a 0.3 m distance, after staying in the 22–23 °C temperature controlled examination room for 15 min, no air flow ($v_{air} < 0.2\ m\ s^{-1}$ - surrounding air speed) and controlled air relative humidity $\varphi < 0.6$ (60%). The subject was asked to remove all facial obstructions (e.g., glasses, front hair fringe, garments). Then the average tympanic temperature, T_{ty}, was measured in both ear canals, using a Braun Thermoscan TIV 3520+, which has a reported accuracy by the manufacturer of ±0.2 °C for the range 36 °C–39 °C, and outside this range ±0.3 °C. However, there are pros and cons of using such devices, therefore, to comply with the necessity of having to measure body temperature to identify patients with fever, not only tympanic temperature was utilized, but also infrared image camera facial temperature as described in the next paragraph. In this way, body temperature measurements were double checked.

For phase 1, individuals were selected from patients who were admitted to the emergency unit of São Paulo University Medicine School Hospital of Clinics. Data were recorded from all admitted patients that were submitted to facial thermal imaging and tympanic temperature, T_{ty}, measurement, between 3 and 68 years old, in the period from 2018 to 2019. The criterion to identify patients with fever was when $T_{ty} > T_{fth} = 37.5\ ^oC$ or $T_{ip} > T_{fth} = 37.5\ ^oC$, in which T_{fth} is the assumed fever threshold temperature, and T_{ip} is the temperature measured by the infrared camera at any image pixel (or position) "ip" on the face. Therefore, for the cases where $T_{ty} \leq 37.5\ ^oC$, but in some image pixel, $T_{ip} > 37.5\ ^oC$, even a single one, the patient was classified in the fever group.

A decision was made to consider only fever cases with viral or bacterial infection contagious lung diseases, previously confirmed by laboratory or imaging exams. All other fever cases were excluded. Then, a second measurement was taken fifteen days after fever treatment. Additionally, cases hospitalized for more than 24 h or undergoing any type of surgical intervention were excluded, as were those with vascular or cutaneous facial disease. In this way, an attempt was made to restrict the group to only individuals with fever originated by respiratory diseases, which is the main characteristic of COVID-19 infections.

Based on the described criteria, the recorded thermal images were classified either in the fever or no fever group and stored in the computer in two folders. In this way, the standard data bank was constructed and made available as input to the CNN algorithm.

2.4. CNN algorithm

As discussed in section 2.2, based on a standard data bank built in

phase 1 of the study, a convolutional neural network (CNN) was used to create three different groups: fever (1), intermediate or subfebrile (2), and no fever (3). For that, an algorithm was devised based on the schematic diagram shown in Fig. 1. The algorithm consisted of splitting the no fever group into two new groups based on the probability of the individual recorded thermal facial image, p_f, to belong to the fever group (1). When $p_f > 0.5$ (50%), the individual was classified in the intermediate or subfebrile group (2), and in the no fever group (3) otherwise.

Fig. 1 shows how the CNN is a layer-based structure, each layer with multiple nodes and each node performing a specific operation, for example, convolution, grouping, loss calculation (Hesamian et al., 2019). The process is composed by an input layer, hidden layers, and an output layer. The hidden layers include layers such as the ones shown in Fig. 1 (feature maps, activation maps, and max pooling) that execute convolutions. The image input goes through a convolutional layer, which converts the visual information to a feature map. The activation layer does multiplication or other dot product, with an activation function, the rectified linear unit (ReLU). The ReLU eliminates negative values from an activation map by attributing zero to them. Next, a pooling step, executes a non-linear down-sampling, which reduces data dimensions through the combination of neuron clusters outputs at one layer into a next layer single neuron. Such step is essential for the CNN to learn features and classify data for images. Two possible ways of doing that are: max and average. In this study, max pooling was utilized, which consists of using each cluster maximum value of neurons at the previous layer.

The nodes of one layer feed the next one with their values. The nodes of the last layer of a neural network represent the output, and the nodes of the first layer the input. In this study, the output is the probability that an image belonged to a certain group, and the input was the image itself.

During the training process, CNN is provided with sample images of each group. As a result, the connection weights for these nodes are adjusted repeatedly to adjust the known output through a back propagation process.

The entries were composed by the facial thermal image, automatically located within the captured image. Hundreds of pixels included the classic maximum skin temperature of the inner canthus area of the eye ($T_{ic,eye}$), average and maximum forehead temperature (T_{fh}), average face temperature, and all possible temperature readings for each pixel on the face and their combination of regions of interest (ROI) from hot and cold areas.

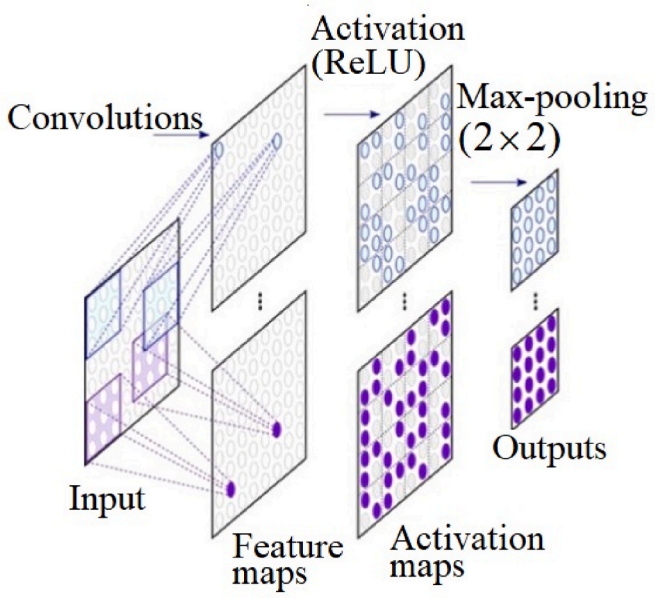

Fig. 1. The layers of the convolutional neural network (CNN) utilized in the study.

The algorithm started with the infrared image input, facial identification within the image, ROI identification, and ROI temperatures comparison with the fever threshold temperature, as shown in Fig. 2. The process then proceeded with an evaluation step by verifying if the maximum facial temperatures ($T_{f,max}$) which comprise all described measured temperatures in the previous paragraph were greater or less/equal than the fever threshold temperature (T_{fth}), primarily identifying fever or no fever groups, respectively. When the subjects did not exceed the fever threshold temperature, i.e., they did not have a fever indication, the image classification algorithm (ICA) classified the thermal image within two fever probability groups: subfebrile (2) if $p_f > 0.5$ (50%), and no fever (3) otherwise, i.e., $p_f \leq 0.5$ (50%). In this way, the method aims at providing an active thermal feature and perhaps new thermograms analysis approach that is expected to be helpful in detecting asymptomatic subjects and those who have intention in suppressing high fever, assuming that ICA could identify abnormal facial vascularization patterns in individuals that did not exceed the fever threshold temperature.

2.5. Prospective study (phase 2)

Phase 2, from April 9 to July 21, 2020, during the COVID-19 pandemic, studied a prospective multicenter population using the herein proposed CNN algorithm to classify the tested subjects as high (1), medium (2), and low (3) risk to be a COVID-19 bearer. The daily

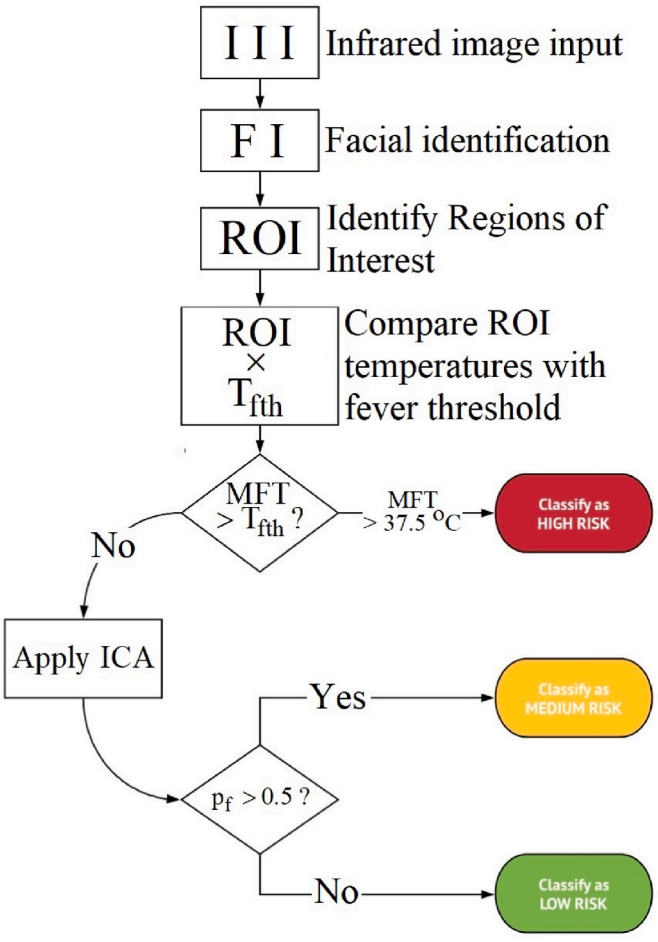

Fig. 2. The CNN algorithm for classification in the fever, subfebrile or no fever group, using the facial infrared image (II). ROI: regions of interest; MFT: maximum facial temperature, and ICA: image classification algorithm.

arrival to work of the tested population was monitored in 73 companies, distributed in Brazil, USA, Mexico, the Netherlands and Lebanon. The image capturing procedure was carried out in the same way as in phase 1 (the retrospective study) but using a rapid infrared image sampling system that was set up in an external, non-thermally controlled environment at the entrance of all selected companies, as shown in Fig. 3 (top). Therefore, it is reasonable to state that the plan could be replicated anywhere in the world due to the simplicity of the hardware required to conduct the tests. The doctor took the facial image with the infrared camera from a window in a separate room, which was then directly processed by the computer with the CNN algorithm to produce the results as shown in Fig. 3 (bottom), either with a green OK to classify the individual in the no fever group or with a red EVALUATE to classify the individual in the fever or subfebrile group. In this way, it is reasonable to state that the method provided a proof of concept of an established active (instead of passive or static) thermal screening method to detect asymptomatic patients and patients who have intention in suppressing high fever, since the subfebrile group was expected to include such individuals. For each subject, the procedure took less than 3 s, with no waiting time, to start the algorithm shown in Fig. 2.

Next, according to the algorithm of Fig. 2, worker admission was granted when the result was low risk (no fever); the worker was guided to clinical evaluation and separation when necessary, in the case of medium risk (intermediate or subfebrile), and the worker was also guided to clinical evaluation followed by separation and isolation when fever was detected (high risk or fever group). In the clinical evaluation, the Center for Diseases Control (CDC) criteria were used to classify the cases as COVID-19 clinically suspicious (fever or chills, cough, shortness of breath or difficulty breathing, fatigue, muscle or body pain, headache, recent loss of taste or smell, sore throat, congested or runny nose, nausea or vomiting, diarrhea) (Center for Disease Control and Prevention, 2020b). Clinical information such as demographic data, smoking history and previous illnesses were recorded. The final diagnosis of COVID-19 was made by real-time reverse transcription polymerase chain reaction (Taylor et al., 2010) (RT-qPCR) using nasopharyngeal swabs.

Fig. 3. Typical rapid infrared image sampling system that was set up in an external, non-thermally controlled environment at the entrance of all selected companies (top). At the bottom 2 examples of the utilized facial infrared images CNN algorithm results are shown either with a green OK (left image) to classify the individual in the no fever group or with a red EVALUATE (right image) to classify the individual in the fever or subfebrile group.

Only cases with clinical evaluation at the time of image capturing were separated for analysis, with medical follow-up for at least 3 months. Conversely, the following cases were excluded from the analysis: i) Cases with poor image quality; ii) Cases in which clinical information or tympanic temperature measurements were not obtained, and iii) People who were sweaty or whose face was hot from previous exposure to excessive heat from the environment or from transportation vehicles.

2.6. Statistical analysis

Data were treated as mean and standard deviation or proportions for continuous or categorical data, respectively. The analysis was performed using the True Epistat statistical software adopting a 95% confidence interval. To estimate the sample size to obtain results with $p < 0.05$, power of at least 80% was considered. Sensitivity/specificity was calculated based on the algorithm's ROC (receiver operating characteristic) curve (Fawcett, 2006) in HCFMUSP cases, which is a graph with the diagnostic ability of a binary classifier system (patient with disease or not) based on the variation of the discrimination threshold. Excel software was also used for COVID-19 suspicious and confirmed clinical data in an external environment. It was assumed a null hypothesis (h0) that there was no association of COVID-19 positive people or clinically suspicious cases with a subfebrile group. The differences between healthy volunteers and patients with and without COVID-19 confirmed infection were analyzed by one-way ANOVA (Analysis of variance), followed by Tukey's post hoc tests or chi-square tests (van Belle, 2008). Subsequently, a random machine learning model was used to perform multivariate analysis of all variables and to categorize patients as positive or negative COVID-19 to identify other factors associated with infrared image in the classification of COVID-19 suspicious cases, considering $p < 0.05$.

3. Results

Phase 1 utilized a total of 1206 selected patients who were admitted to the emergency room, from which 630 were men (52.2%), 32 ± 12 years old. In the sample, 156 were fever cases of pulmonary origin (15%), from which 78 were men, 20 ± 7 years old, with $T_{ty} = 38.90 \pm 0.68$ °C, who were eligible. All of them recovered from fever within 2 weeks, registering $T_{ty} = 36.12 \pm 0.49$ °C, and served as control for the development of the CNN algorithm. The ROC curve showed 97.8 and 98% sensitivity and specificity, respectively, due to the substantial temperature differences between the fever and no fever groups.

After the creation of the CNN algorithm, phase 2 carried out 227,261 workers evaluations during the daily arrival to work at the entrance of 73 companies in 23 cities in 5 countries, lasting 103 days. The companies' distribution per countries was: 51.5% in Brazil, 39% in Mexico, 9% in the USA, 0.2% in Lebanon and 0.02% in the Netherlands. The companies were in 8 states in Brazil (south, southeast, midwest and north regions). There was an average of 3113 tests per company.

Based on the methodology described in section 2, using the standard data bank built in phase 1, phase 2 results allowed for the classification of the tested individuals in three groups to identify possible COVID-19 bearers: 1) fever (high risk); 2) intermediate or subfebrile (medium risk), and 3) no fever (low risk). In sum, 7605 fever (high risk) cases (3.3%) and 31,173 subfebrile/intermediate (medium risk) cases (13.7%) were identified. The remaining subjects were classified with no fever (low risk), i.e., thermally normal. The distribution pattern was approximately the same, with no significant difference in incidence between countries or even over the 103 days ($p > 0.05$), as summarized

graphically in Fig. 4.

The CNN algorithm was capable of clearly distinguishing three groups based on facial infrared images temperature distribution differences. However, using the three-group classification obtained with the CNN algorithm for the set of 227,261 tested individuals, it was possible to demonstrate that based only on the comparison between maximum skin temperature of the inner canthus area of the eye, $T_{ic,eye,max}$, and average forehead temperature, $T_{fh,avg}$, or both, it was not possible to classify the same tested individuals in the three groups. Indeed, with $T_{ic,eye,max}$ and $T_{fh,avg}$ there were no significant differences in the individuals measured temperatures comparison, i.e., the measured temperature ranges overlapped in the three groups ($p > 0.05$). Fig. 5 shows the results of the analysis as follows: i) The bars indicate the number of cases in each temperature interval; ii) The solid lines represent the bars normal distributions; iii) The vertical axis indicates the number of tested individuals, N_{ti}, from the total of tested individuals, $N_{ti,tot} = 227,761$, and iv) The horizontal axis shows a graded temperature scale (1 °C intervals) that depicts $T_{fh,avg}$ and $T_{ic,eye,max}$ in Fig. 5a and b, respectively. Therefore, Fig. 5 shows graphically the statistical test results that allowed for the conclusion that based only on the measured $T_{fh,avg}$ and $T_{ic,eye,max}$ it was not possible to classify the tested individuals in fever, subfebrile and no fever groups since $p > 0.05$ (Pearson p-value test) (van Belle, 2008).

In the examination sites, the external (ambient) temperature, T_∞, varied from −3.4 °C to + 35.9 °C, so that $\overline{T}_\infty \pm 2\sigma_{T_\infty} = 20.40 \pm 6.02$ °C, and the relative humidity, $\overline{\varphi} \pm 2\sigma_\varphi = 68.70 \pm 10.50\%$. The statistical analysis allowed for concluding that there was no relationship between ambient temperature (maximum, average, minimum), relative humidity or wind speed with the maximum eye temperature, average forehead temperature, or risk classification by the algorithm ($p > 0.05$). Only the average skin temperature was weakly affected by the minimum external temperature ($p = 0.316$). All other relationships were negligible. Hence, there was no need to correlate facial infrared image temperature values to those of the local weather for data analysis. Neither sensitivity nor specificity had significant differences with respect to the tested environment.

After the initial infrared image exams with 227,261 tested individuals, only a total of 2558 complete cases were eligible to be analyzed with an average follow-up of 3.5 months (3–6 months variation), from the 73 companies that participated of the study. The no fever group amounted to 2283 cases (89.2%), the subfebrile group 264 cases (10.3%) and the fever group 11 cases (0.43%). The reason for not using

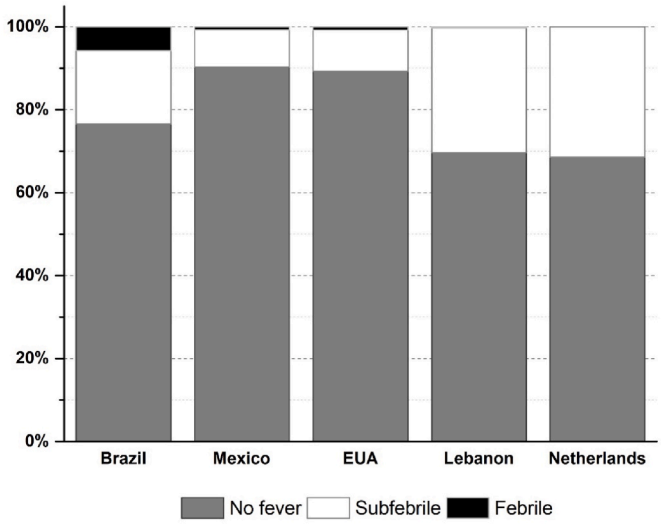

Fig. 4. Percentage comparison of no fever, subfebrile and fever cases in Brazil, Mexico, USA, Lebanon and The Netherlands, for 103 days.

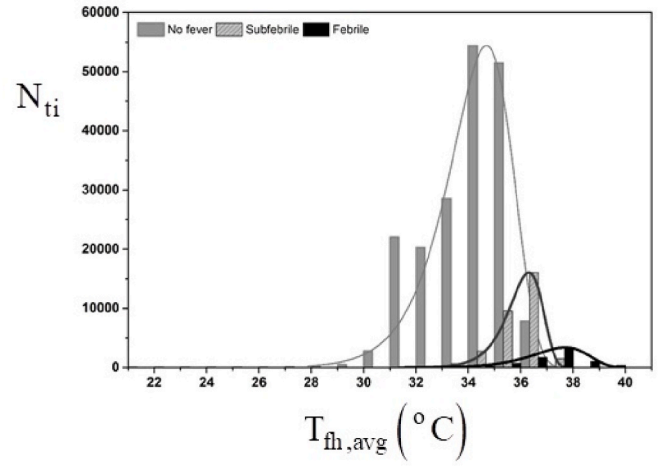

(a)

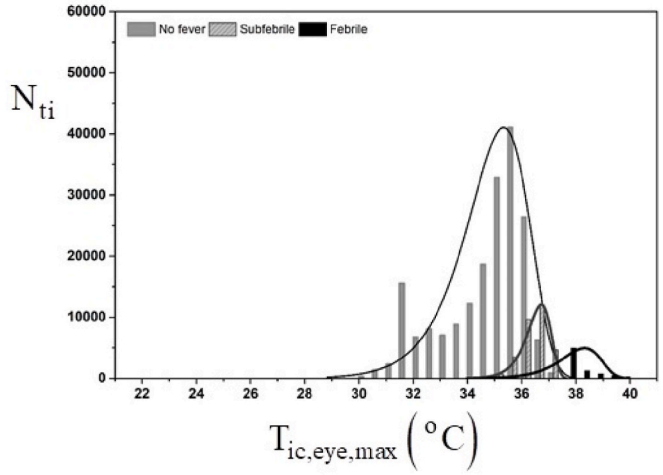

(b)

Fig. 5. Distribution of temperatures in the no fever, subfebrile and fever groups for 103 days; a) average forehead temperature, and b) maximum eye temperature. The bars indicate the number of cases in each temperature interval; ii) The solid lines represent the bars normal distributions; iii) The vertical axis indicates the number of tested individuals (N_{ti}).

the other tested individuals in the original sample was that clinical or laboratory follow-up with RT-qPCR or subsequent contact was not possible since the workers could not be reached because they were only visiting the company or were referred to other medical services. Most eligible cases were men in the three groups (92.8%) with a 31-year-old mean with an age range from 18 to 71 years old. In the group, 56 suspected cases that had any of the COVID-19 symptoms, including fever or not (80.3% subfebrile, 45 cases) were found, 19 of which were confirmed with RT-qPCR for COVID-19, who were directed to isolation for 14 days. In the subfebrile (intermediate) group, Table 1 shows two cases that had to be hospitalized in severe condition for 8 and 10 days due to low saturation ($SaO_2 < 88\%$), with pulmonary sequelae in 25 and 50% of the lung area (tomography), respectively. There were no deaths among the COVID-19 confirmed cases.

As stated in the previous paragraph, the complete evaluation was undertaken with 2558 individuals. From the 45 subfebrile cases selected by the CNN algorithm, 17 subjects were confirmed with RT-qPCR for COVID-19, as it is shown in Table 1.

Table 2 shows that the addition of the subfebrile to the fever group to establish the COVID-19 suspicious cases increased the screening

Table 1
Compilation of COVID-19 free, symptomatic, RT-qPCR confirmed, and hospitalized cases.

Group	N (%)	Symptomatic	RT-qPCR confirmed	Hospitalized cases
No fever	2283 (89.3%)	0	0	0
Subfebrile	264 (10.3%)	45 (80.4%) *	17 (89.5%) *	2 (100%) *
Fever	11 (0.4%)	11 (19.6%)	2 (10.5%)	0
Total	**2558**	**56**	**19**	**2**

*$p < 0.01$.

Table 2
Statistical parameters of the COVID-19 diagnosis CNN algorithm.

Group	Parameter	RT-qPCR positive	RT-qPCR negative
Fever Group (N = 11)	**Fever Algorithm**	2	9
	No fever Algorithm	17	2530
	Sensitivity:	0.1053	CI: 0.0294 to 0.3139
	Specificity:	0.9965	CI: 0.9933 to 0.9981
	Accuracy:	98.98%	
	PPV	18.18%	
	VPN	99.33%	
Subfebrile Group (N = 264)	**Subfebrile Algorithm**	17	247
	Non-Subfebrile Algorithm	2	2292
	Sensitivity:	0.8947	CI: 0.6861 to 0.9706
	Specificity:	0.9027	CI: 0.8906 to 0.9136
	Accuracy:	90.27%	
	PPV	6.44%	
	NPV	99.91%	
Subfebrile + Fever Groups (N = 275)	**Fever or Subfebrile Algorithm**	19	256
	No fever Algorithm	0	2283
	Sensitivity:	1.0000	CI: 0.8318 to 1.0000
	Specificity:	0.8992	CI: 0.8869 to 0.9103
	Accuracy:	89.99%	
	PPV	6.90%	
	NPV	100.00%	

CI: Confidence Interval, PPV: Positive Predictive Value, NPV: Negative Predictive Value.

sensitivity from 0.1053 (fever group) to 1.000 (fever + subfebrile group), taking the lower limit of the confidence interval. Note that the fever group was formed with screening based only on temperature greater than 37.5 °C (fever group), as presented in section 2.3. Hence, the CNN algorithm could detect substantially more confirmed COVID-19 cases than the fever screening criterion based on the temperature threshold only. Indeed, the fever + subfebrile group included all 19 confirmed COVID-19 cases in the sample.

Regarding associated signs and symptoms to COVID-19, according to the CDC (Center for Disease Control and Prevention, 2020b), Table 3 shows that in the subfebrile group substantially more signs and symptoms were found than in the fever group, either in the COVID-19 (−) or COVID-19 (+) individuals. Remarkably, in the subfebrile group, the COVID-19 CDC criteria symptoms were prevalent in the COVID-19 (−) cases, which in the current study were caused by other simple flu conditions and related illnesses. Therefore, COVID-19 characteristic symptomatic cases were more detected in the COVID-19 (−) than in the COVID-19 (+) evaluated subjects in the subfebrile group.

Table 3
Signs and symptoms in the fever and subfebrile groups.

Associated Signs and Symptoms[55]	Subfebrile (N = 45)		Fever (N = 11)	
	COVID-19 (−) (N = 28)	COVID-19 (+) (N = 17)	COVID-19 (−) (N = 9)	COVID-19 (+) (N = 2)
Anosmia	3 (6.6%)	1 (5.9%)	0	0
Coryza	18 (40%)	3 (17.6%)	0	0
Headache	15 (33.3%)	0	1 (9%)	0
Odynophagia	9 (20%)	2 (11.8%)	0	0
Myalgia	14 (31.1%)	0	0	0
Diarrhea	3 (6.6%)	1 (5.9%)	0	0
Cough	6 (13.3%)	5 (29.4%)	0	0
Fatigue	2 (4.4%)	1 (5.9%)	0	0
Nausea/vomiting	3 (6.6%)	2 (11.8%)	0	0
Tachycardia >100 bpm	16 (35.5%)	0	1 (9%)	0
Bradycardia <50 bpm	3 (6.65%)	1 (5.9%)	0	0
Sun exposure [a]	15 (33.3%)	2 (11.8%)	0	0
Sleep deprivation	16 (35.5%)	0	1 (9%)	0
Total number of occurrences	**123**	**18**	**3**	**0**

[a] Exposed to sun irradiation all day long outdoors.

Additionally, in the fever group, the 2 COVID-19 (+) cases did not present symptoms other than fever itself, but the 9 COVID-19 (−) cases showed a total of 3 occurrences of COVID-19 CDC criteria symptoms (Center for Disease Control and Prevention, 2020b).

In Table 3, it should be noted that some individuals were polysymptomatic, i.e., presented one or more symptoms, and others no symptoms at all. The last row shows the total number of occurrences of signs/symptoms in each group. For example, 123 occurrences of signs or symptoms were detected in the 28 COVID-19 (−) subfebrile cases. Note also that cough was the most common symptom in the 17 COVID-19 (+) subfebrile cases (29.4%).

Table 4 shows the 56 symptomatic cases classified either as COVID-19 (−) or COVID-19 (+). For that, the 45 symptomatic cases that belonged to the subfebrile group (264 cases) and the 11 cases of the fever group were combined. The total number of occurrences of symptoms in each column shows that 19 COVID-19 (+) and 37 COVID-19 (−) individuals had 20 and 135 types of symptoms, respectively, now including fever, which is one of the COVID-19 CDC criteria symptoms (Center for Disease Control and Prevention, 2020b). The main reason for presenting Table 4 results is the observation that polysymptomatic individuals appeared more in the COVID-19 (−) cases than in the COVID-19 (+) cases, thus allowing to discard the occurrence of

Table 4
Symptoms comparison between COVID-19 (+) and COVID-19 (−) individuals.

Associated Symptoms	COVID-19 (+) N = 19	COVID-19 (−) N = 37
Fever (N = 11)	2 (10.5%)	9 (24.3%)
Subfebrile (N = 45)	17 (89.4%)	28 (75.6%)
Anosmia	1 (5.3%)	3 (8.1%)
Coryza	3 (15.8%)	18 (48.6%) *
Headache	0	16 (43.2%) *
Odynophagia	2 (10.5%)	9 (24.3%) **
Myalgias	0	14 (37.8%) *
Diarrhea	1 (5.3%)	3 (8.1%)
Cough	5 (26.3%)	6 (16.2%)
Fatigue	1 (5.3%)	2 (5.4%)
Nausea/vomiting	2 (10.5%)	3 (8.1%)
Tachycardia >100 bpm	0	17 (45.9%) *
Bradycardia <50 bpm	1 (5.3%)	3 (8.1%)
Sun exposure ***	2 (10.5%)	15 (40.5%) **
Sleep deprivation	0	17 (45.9%) *
Fever	2 (10.5%)	9 (24.3%)
Total number of occurrences	**20**	**135**

*$p < 0.01$, **$p < 0.05$, *** exposed to sun irradiation all day long outdoors.

simultaneous symptoms as a clear indication of COVID-19 infection, at least in the sample herein analyzed.

The fever and subfebrile groups' results were combined to depict a global picture of the 2558 complete cases in terms of clinical signs such as runny nose, tachycardia, headache, myalgia and odynophagia and sun exposure. The signs/symptoms were not exclusive to the confirmed cases of COVID-19. However, they were significantly present only in the 56 individuals clinically suspect group that was analyzed through the results shown in Tables 3 and 4 Furthermore, the 19 COVID-19 (+) cases were all symptomatic in the 2558-case tested sample. Hence, no asymptomatic COVID-19 (+) cases were detected in the sample.

The study proceeded with the demographic comparison between COVID-19 (+) and COVID-19 (−) individuals shown in Table 5. The results investigate the correlation between age, and several other suspected associated factors with COVID-19 (+) cases in the 2558-case tested sample. Clearly, older individuals were more affected than younger ones. Indeed, the COVID-19 (+) group averaged 45.3 years old whereas the COVID-19 (−) group averaged 30.55 years old, i.e., 48.3% older than the COVID-19 (−) group. Therefore, age was confirmed as a high-risk factor for COVID-19 infection. Most other investigated conditions (obesity, overweight, normal weight, diabetes, no fever, subfebrile, fever, smoker, asthma/chronic obstructive pulmonary disease – COPD, systemic arterial hypertension – SAH, pregnant, and heart disease) appear not to be of major importance for increased COVID-19 (+) risk, from the number of cases listed in Table 5, except for the subfebrile condition that was found to be related to 17 of the 19 COVID-19 (+) cases identified in the sample. Hence, it is reasonable to state that Table 5 results clearly indicate that the subfebrile condition detected by the herein proposed CNN algorithm was shown to be of great importance for possible COVID-19 (+) individuals screening.

4. Discussion

In this study, it was possible to identify, by means of mass screening, a subfebrile (intermediate) group that was shown to be related to COVID-19 (+) cases through the evaluation of 2558 cases through the combination of infrared imaging and a herein proposed CNN algorithm, and use it as an unprecedented screening variable. Ideally, a screening method should be simple, fast, and overly sensitive, characteristics that have been obtained with the herein proposed methodology through experimental results.

A final and precise diagnosis is not what is sought by a screening technique. However, the method needs to be shown useful in separating suspicious cases in large crowds, so that disease spread, and contagion are avoided. Although thermography has been widely utilized for COVID-19 screening for air travel and access to public places, the method has not been soundly effective in identifying suspicious COVID-19 (+) individuals, as shown by the technical literature (Chiang et al., 2008; Ng and Acharya, 2009; Ng and Kee, 2008; Zhou et al., 2020), which motivates the development of viable alternatives to improve effectiveness of the method. Towards that goal, the herein proposed methodology is the first to propose the separation and analysis of a subfebrile group during people infrared screening. For that, the group characteristics, incidence, and clinical importance had to be assessed and experimentally related to COVID-19 (+) individuals, which was done for the first time through infrared imaging and COVID-19 RT-qPCR tests.

A subfebrile state is quite difficult to be defined, since there is no consensus on fever threshold, which varies according to the place and means of assessment (Coats et al., 2018; Jessen, 1985; Nishiura and Kamiya, 2011; Sun et al., 2017; Tan and Knight, 2018). In this study, the subfebrile state was defined as cases with a facial temperature <37.5 °C and more than 50% probability of being fever according to the facial CNN algorithm. In this way, the thermographic analysis considered the facial temperature distribution by evaluating multiple thermal points, and not just a single point as it is common practice. Most published articles use maximum skin temperature of the inner canthus of the eye temperature or average forehead temperature, i.e., always with one or a few points of analysis (Center for Disease Control and Prevention, 2020b; Fawcett, 2006; Fitriyah et al., 2017; Hesamian et al., 2019; Hewlett et al., 2011; Liu et al., 2004, 2020; NG et al., 2005; Ng and Kee, 2008; Nguyen et al., 2010; Taylor et al., 2010; U.S. Department of Health and Human Services et al., 2020). Within the knowledge of the authors, this is the first study to assess all facial thermal points simultaneously. The herein obtained results showed a clear overlap of the normal, subfebrile, and fever classification when using fixed temperature values, which decreases the sensitivity of screening specificity.

The clear overlap of the normal, subfebrile, and fever classification using only the maximum skin temperature of the inner canthus of the eye temperature or average forehead temperature was shown in Fig. 5. A possible physical explanation for the results of Fig. 5 is that since an individual should be included in the fever group when even one $T_{ip} > 37.5$ °C, if $T_{ic,eye,max}$ is utilized, one possible $T_{ip} > 37.5$ °C could be missed because the MFT does not need to be specifically in the eye. Such point could be in other facial point, which does not go "unnoticed" with the CNN algorithm, that includes all facial points. Hence, the objective of showing the results of Fig. 5 was to demonstrate that using only measurements of $T_{fh,avg}$ and $T_{ic,eye,max}$ would not be enough to produce the same group classification obtained with the herein proposed CNN algorithm.

As stated in the proposed methodology, the fever cases were identified in this study by the feverish face characterized by a thermal signature (based on the facial temperature distribution) automatically by artificial intelligence. The change with respect to the expected normal facial temperature distribution may be related to a systemic inflammatory condition by interleukin IL-6 and ultrasensitive C-reactive protein (hs-PCR) caused by viral or bacterial pyrogens (Alheim et al., 1997; Benarroch, 2007; Blatteis, 2006; Coomes and Haghbayan, 2020; Liu et al., 2020; McGonagle et al., 2020; Rodríguez-Medina, 2018), generating an increase in the flow of vascular springs – supraorbital region – angular and labial) and vasoconstriction in the extremities (nose, cheeks and chin) (Blatteis, 2006; Cruz-Albarran et al., 2020; Rodríguez-Medina, 2018). Fever happens when the hypothalamus detects pyrogens and then increases the set point. The course of typical fever can be divided into three stages. When the fever starts, the body tries to increase its temperature, but vasoconstriction occurs to prevent heat loss through the skin. For this reason, some individuals in this fever stage (in the upward slope and immediately after the onset of the fever

Table 5
Demographic comparison between COVID-19 (+) and COVID-19 (−) individuals.

Variable	COVID-19 (−) (N = 2549)	COVID-19 (+) (N = 19)
$\bar{a} \pm 2\sigma_a$ (95% of the population)	30.55 ± 28.46	45.30 ± 27.08
Gender (%)	M = 2319 (91.2%), F = 220 (8.64%)	M = 15 (81.2%), F = 4 (18.8%)
Obesity (BMI ≥ 35)	139 (5.46%)	2 (10.5%)
Overweight (25 ≤ BMI < 35)	383 (15.04%)	1 (5.2%)
Normal BMI (18 ≤ BMI < 25)	522 (20.49%)	3 (15.7%)
Diabetes	24 (0.9%)	1 (5.2%)
No fever	2283 (89.63%) *	0
Subfebrile	28 (1.1%)	17 (89.5%) *
Fever	9 (0.35%)	2 (10.5%) *
Smoker	179 (7.03%)	3 (1.17%)
Asthma/COPD	128 (5.03%)	0
Systemic arterial hypertension (SAH)	281 (11.03%)	1 (5.2%)
Pregnant	3 (0.12%)	0
Heart disease	102 (4.00%)	0

*p < 0.01, BMI: body mass index, COPD: Chronic obstructive pulmonary disease, M: male, F: female.

or in the downward slope after the onset of the fever) will not be detected by conventional thermography (Ng et al., 2006). The measurement of these inflammatory proteins should be better studied to understand their influence on thermographic evaluation.

A multicenter, observational, cohort study (without intervention) was carried out in two stages — hospital and population, respectively — in which it was possible to assess regions of different climates and locations, and the demographic profile of those evaluated was similar to that studied in most previously published studies (Boehmer et al., 2020; Omori et al., 2020; Venkatesan, 2020; Wedderburn et al., 2020). The herein obtained experimental results, as in the technical literature, showed a low fever incidence, which was less than 1–3% (Canadian Agency for Drugs and Technologies in Health, 2014; Ring et al., 2013). The algorithm could be used both indoors and outdoors. Although the study was based on measurements taken in a controlled environment, unlike the literature, any significant interference of the ambient temperature in the analysis of the results was not detected. A possible physical explanation to that fact is that the dynamic balance of heat production, transfer and loss of various locations of the head in living human beings is a complex process (even more so, with extra work by the moving subject) in which the physiological mechanisms are continuously in action to maintain body temperature (Ng et al., 2006; Pascoe, 2010).

The proposed CNN algorithm enhanced infrared imaging procedure would allow for creating a database and a real time information control center that could pinpoint locations at high risk (e.g., places with high incidence of fever or subfebrile cases), so that other public restrictive measures would be guided and taken in the population exposed to the virus, and even priority vaccination measures. A 3-day mobile mean could be utilized to create an alert tracking of possible increase in cases, before RT-qPCR tests are available, and also symptomatic cases. The greater the number of thermographic alerts for fever and subfebrile cases, the greater the viral exposure during the epidemic period and, therefore, the greater contagion risk would be expected in each company. Such assertion was made on solid ground, i.e., based on the results of this study, in which 19 of 275 cases (6.9%) screened from a sample of 2558 cases belonged to the fever (11 cases) and subfebrile groups (264 cases), and were COVID-19 (+). Noteworthy is that all 19 COVID-19 (+) cases detected in the 2558 individuals' sample (0.7% ~ 1%) by RT-qPCR tests were among the screened individuals as part of the fever and subfebrile groups.

The herein proposed method is therefore an inexpensive and easy method to be implemented for the COVID-19 general population mass evaluation that probably would not miss positive cases without fever, which has been the case with conventional thermography. In this study, the subfebrile group brought 264 people for further investigation who would undergo conventional thermal screening without clinical evaluation, from which 17 were confirmed COVID-19 (+) (6.4%), thus the method increased the noninvasive identification of COVID-19 (+) cases, and in fact was capable of screening all COVID-19 (+) cases present in the sample that were later confirmed by RT-qPCR tests.

The standard data bank construction (Phase 1) was based on 1206 hospital emergency unit selected patients, which was a sample size sufficient to build the algorithm, representative and homogeneous. For the prospective study (Phase 2), although the tests were carried out in a multicenter study, they were targeted to an active workers population, not in isolation, and predominantly middle-aged men. In addition, the authors were rigorous in selecting the cases, excluding many that clinical follow-up was not possible.

Since the tests were not a comparative study between locations with and without the use of the algorithm, it is not possible to state that they could restrict a pandemic, but based on the obtained results, it is reasonable to state that they were more effective than just screening people with fever. The multi-point thermography of the face was also demonstrated to be more effective than the analysis of the maximum temperature of the eyes or forehead, used in conventional thermography.

The medical costs both to employers and the medical health systems associated with leave of absence from work and hospitalization can be very high. For example, in Brazil, each employee on leave costs more than US$1100 and when hospitalized more than US$3500 to the employer. In this study, employees identified as subfebrile were active on their way to work but were immediately removed for treatment without the need for hospitalization after early clinical confirmation. Therefore, it is reasonable to state that, potentially, the methodology would lead to a cost reduction of more than US$3500 per hospitalized person identified early by the algorithm as subfebrile. Only 2 of 17 in the subfebrile group (12%) were hospitalized. In addition, none of the 11 fever patients required hospitalization (mild/moderate infection).

Some limitations of the study could be pointed out. Since it was a population screening study, it was not possible to previously separate other pre-existing clinical conditions or use of medications. Therefore, many of the results classified as subfebrile may be related not only to other non-viral infectious diseases, but also to systemic diseases such as hypertension, allergy, facial acne, and extrinsic factors such as heat stroke, sleep deprivation, alcohol or use of vasoactive medications. However, all such variables could be quickly assessed in the initial clinical approach after thermal alert. Furthermore, since COVID-19 (+) asymptomatic cases were not detected in the 2558 sample tested in this study, it was not possible to verify the sensitivity of the subfebrile group screening to detect possible COVID-19 (+) asymptomatic cases.

This study contributed to COVID-19 subclinical screening and possibly other communicable viruses. The study dealt with the unprecedented evaluation of subfebrile cases with COVID-19, by means of multicentric mass tracking in different countries, using infrared imaging coupled to an artificial intelligence algorithm for the selection of potentially COVID-19 infected non-febrile individuals. Currently, there is great global public interest in the topic of finding novel, alternative and affordable methodologies for effective pandemics control. In that sense, the study brought to light a more specific possibility regarding the tracking of fever and subfebrile cases that had not yet been reported in the technical literature, and that stimulates new research and ideas for the scientific community to proceed in this line of investigation. Despite this study's promising results, exercising caution is needed when issuing a final recommendation. The predictive value of infrared imaging is likely to vary depending on the natural course of the disease and a variety of other environmental factors. Therefore, more extensive studies are needed to confirm the findings of this study, and possible validation by other authors. One possible direction would be to test the algorithm with only confirmed COVID-19 (+) cases, with and without fever.

5. Conclusion

The key conclusions of this study were.

1. It was possible to identify suspicious and confirmed COVID-19 (+) cases characterized by temperatures below the 37.5 °C fever threshold by means of a CNN algorithm enhanced infrared imaging procedure to evaluate multiple thermal points on the face.
2. It was shown that only measurements of $T_{fh,avg}$ and $T_{eye,max}$ greater than 37.5 °C, which is the traditional thermography method for fever classification, would not be enough to produce the fever group classification obtained with the herein proposed CNN algorithm, since the MFT could be in a facial point neither in the eye nor in the forehead.
3. The incidence of fever in the 227,261 screening at the entrance of the subjects' place of work was low (3.3%), but most of 19 COVID-19 (+) cases found in a 2558 cases sample, including hospitalization, belonged to the subfebrile group (17 cases/89.5%) and not to the fever group.
4. Regarding RT-qPCR confirmed COVID-19 (+) cases, the main risk factor was found to be part of the screened subfebrile group, followed

by age, with had a 45.3-year-old mean in comparison to a 30.55-year-old mean for COVID-19 (−) cases (48.3% higher). Other risk factors were investigated and found to be much less significant than the two main risk factors, such as diabetes, high blood pressure and smoking.
5. Clinical signs of runny nose, tachycardia, headache, myalgia and odynophagia, although present in the suspicious cases, were not exclusive to the COVID-19 (+) group;
6. The subfebrile and fever groups screened by the herein proposed CNN algorithm was shown to be of great importance for possible COVID-19 (+) individuals screening, since all 19 COVID-19 (+) cases detected in this study for the 2558 individuals' sample (0.7% ~ 1%) by RT-qPCR tests were among the screened individuals as part of the fever and subfebrile groups.
7. Follow-up studies are needed to confirm the findings of this study, and possible validation by other authors. One possible direction would be to test the algorithm with only confirmed COVID-19 (+) cases, with and without fever.

CRediT authorship statement

Marcos Leal Brioschi: Conceptualization, Methodology, Formal analysis, Investigation, Resources, Data Curation, Writing - Original Draft, Writing - Review & Editing, Visualization, Supervision, Project administration. **Carlos Dalmaso Neto:** Conceptualization, Methodology, Investigation, Data Curation, Writing - Original Draft, Writing - Review & Editing, Visualization. **Marcos de Toledo:** Investigation, Resources, Data Curation. **Eduardo Borba Neves:** Methodology, Formal analysis, Data Curation, Writing - Review & Editing. **José Viriato Coelho Vargas:** Writing - Review & Editing, Visualization, Supervision. **Manoel Jacobsen Teixeira:** Writing - Review & Editing, Supervision.

Ethical approval

This retrospective cross-sectional analysis of the IT database of cases admitted to an emergency unit (Hospital of Clinics, Faculty of Medicine, University of São Paulo, Brazil) was reviewed and approved by an Ethics Committee and did not require informed consent.

Funding sources

The authors acknowledge with gratitude the support of the Brazilian National Council of Scientific and Technological Development, CNPq, project 313646/2020–1.

Declaration of competing interest

We declare that we have no conflict of interests.

Acknowledgements

The authors acknowledge with gratitude the support of the Brazilian National Council of Scientific and Technological Development, CNPq, project 313646/2020–1; the cooperation of the Hospital of Clinics, Faculty of Medicine, University of São Paulo, Brazil, and the contribution of João Pedro Rusisca de Toledo (Brazil), Mayco Anderson Guedes Maciel Moreira (Brazil), Barry R. Hix (USA/Mexico), Irma Wensink (Netherlands) and Saad M. Halimi (Lebanon) who supplied infrared image data to this study.

Appendix A. Supplementary data

Supplementary data to this article can be found online at https://doi.org/10.1016/j.jtherbio.2022.103444.

References

Alheim, K., Chai, Z., Fantuzzi, G., Hasanvan, H., Malinowsky, D., Di Santo, E., Ghezzi, P., Dinarello, C.A., Bartfai, T., 1997. Hyperresponsive febrile reactions to interleukin (IL) 1 and IL-1 , and altered brain cytokine mRNA and serum cytokine levels, in IL-1 -deficient mice. Proc. Natl. Acad. Sci. USA 94, 2681–2686. https://doi.org/10.1073/pnas.94.6.2681.

Antabak, A., Sisko, J., Romić, I., Papes, D., Pasini, M., Haluzan, D., Bogović, M., Medancić, S.S., Cavar, S., Luetić, T., Fuchs, N., Andabak, M., Prlić, I., Curković, S., 2016. [FRONTAL, axillary and tympanic temperature measurements in children]. Lijec. Vjesn. 138, 30–33.

Arons, M.M., Hatfield, K.M., Reddy, S.C., Kimball, A., James, A., Jacobs, J.R., Taylor, J., Spicer, K., Bardossy, A.C., Oakley, L.P., Tanwar, S., Dyal, J.W., Harney, J., Chisty, Z., Bell, J.M., Methner, M., Paul, P., Carlson, C.M., McLaughlin, H.P., Thornburg, N., Tong, S., Tamin, A., Tao, Y., Uehara, A., Harcourt, J., Clark, S., Brostrom-Smith, C., Page, L.C., Kay, M., Lewis, J., Montgomery, P., Stone, N.D., Clark, T.A., Honein, M. A., Duchin, J.S., Jernigan, J.A., 2020. Presymptomatic SARS-CoV-2 infections and transmission in a skilled nursing facility. N. Engl. J. Med. 382, 2081–2090. https://doi.org/10.1056/NEJMoa2008457.

Atkins, E., Bodel, P., 1972. Fever. N. Engl. J. Med. 286, 27–34. https://doi.org/10.1056/NEJM197201062860109.

Bai, Y., Yao, L., Wei, T., Tian, F., Jin, D.-Y., Chen, L., Wang, M., 2020. Presumed asymptomatic carrier transmission of COVID-19. JAMA 323, 1406. https://doi.org/10.1001/jama.2020.2565.

Benarroch, E.E., 2007. Thermoregulation: recent concepts and remaining questions. Neurology 69, 1293–1297. https://doi.org/10.1212/01.wnl.0000275537.71623.8e.

Bernardo, L.M., Henker, R., O'Connor, J., 1999. Temperature measurement in pediatric trauma patients: a comparison of thermometry and measurement routes. J. Emerg. Nurs. 25, 327–329. https://doi.org/10.1016/S0099-1767(99)70063-2.

Bhat, T.A., Kalathil, S.G., Bogner, P.N., Blount, B.C., Goniewicz, M.L., Thanavala, Y.M., 2020. SARS-CoV-2 viral load in upper respiratory specimens of infected patients. N. Engl. J. Med. 382, 1175–1177. https://doi.org/10.1056/NEJMc2000231.

Biomedical and Health Standards Committee, 2020a. Specification for Thermal Imagers for Human Temperature Screening – Part 1: Requirements and Test Methods.

Biomedical and Health Standards Committee, 2020b. Specification for Thermal Imagers for Human Temperature Screening – Part 2: Implementation Guidelines.

Bitar, D., Goubar, A., Desenclos, J.C., 2009. International travels and fever screening during epidemics: a literature review on the effectiveness and potential use of non-contact infrared thermometers. Euro Surveill. 14.

Blatteis, C.M., 2007. The onset of fever: new insights into its mechanism. In: Progress in Brain Research, pp. 3–14. https://doi.org/10.1016/S0079-6123(06)62001-3.

Blatteis, C.M., 2006. Endotoxic fever: new concepts of its regulation suggest new approaches to its management. Pharmacol. Ther. 111, 194–223. https://doi.org/10.1016/j.pharmthera.2005.10.013.

Boehmer, T., DeVies, J., Caruso, E., van Santen, K., Tang, S., Black, C., Hartnett, K., Kite-Powell, A., 2020. Changing age distribution of the COVID-19 pandemic. Morb. Mortal. Wkly. Rep. 69, 1404–1409.

Brioschi, M.L., Eduardo, J., Matias, F., Teixeira, M.J., Vargas, J.V.C., 2010. Automated computer diagnosis of IR medical imaging. InfraMation 10.

Canadian Agency for Drugs and Technologies in Health, 2014. Mass Thermography Screening for Infection and Prevention: A Review of the Clinical Effectiveness (CADTH Rapid Response Reports).

Center for Disease Control and Prevention, 2020a. Screening clients for COVID-19 at homeless shelters or encampments [WWW Document]. URL. https://www.cdc.gov/coronavirus/2019-ncov/community/homeless-shelters/screening-clients-respiratory-infection-symptoms.html.

Center for Disease Control and Prevention, 2020b. Interim clinical guidance for management of patients with confirmed coronavirus disease. COVID-19) [WWW Document]. URL. https://www.cdc.gov/coronavirus/2019-ncov/hcp/clinical-guidance-management-patients.html.

Chan, L.-S., Cheung, G.T.Y., Lauder, I.J., Kumana, C.R., 2006. Screening for fever by remote-sensing infrared thermographic camera. J. Trav. Med. 11, 273–279. https://doi.org/10.2310/7060.2004.19102.

Cheung, B.M.Y., Chan, L.S., Lauder, I.J., Kumana, C.R., 2012. Detection of body temperature with infrared thermography: accuracy in detection of fever. Hong Kong Med. J. 18 (Suppl. 3), 31–34.

Chiang, M.-F., Lin, P.-W., Lin, L.-F., Chiou, H.-Y., Chien, C.-W., Chu, S.-F., Chiu, W.-T., 2008. Mass screening of suspected febrile patients with remote-sensing infrared thermography: alarm temperature and optimal distance. J. Formos. Med. Assoc. 107, 937–944. https://doi.org/10.1016/S0929-6646(09)60017-6.

Chiappini, E., Sollai, S., Longhi, R., Morandini, L., Laghi, A., Osio, C.E., Persiani, M., Lonati, S., Picchi, R., Bonsignori, F., Mannelli, F., Galli, L., de Martino, M., 2011. Performance of non-contact infrared thermometer for detecting febrile children in hospital and ambulatory settings. J. Clin. Nurs. 20, 1311–1318. https://doi.org/10.1111/j.1365-2702.2010.03565.x.

Childs, C., 2018. Body temperature and clinical thermometry. In: Handbook of Clinical Neurology. Elsevier B.V., pp. 467–482. https://doi.org/10.1016/B978-0-444-64074-1.00029-X

Chiu, W., Lin, P., Chiou, H.Y., Lee, W.S., Lee, C.N., Yang, Y.Y., Lee, H.M., Hsieh, M.S., Hu, C., Ho, Y.S., Deng, W.P., Hsu, C.Y., 2005. Infrared thermography to mass-screen suspected sars patients with fever. Asia Pac. J. Publ. Health 17, 26–28. https://doi.org/10.1177/101053950501700107.

Coats, T.J., Morsy, M., Naseer, S., Keresztes, K., Hussain, S., Dexter, K., Sims, M.R., 2018. A pilot study of the Leicester ED medical infrared imaging protocol in fever and sepsis. PLoS One 13. https://doi.org/10.1371/journal.pone.0201562.

Conti, B., 2004. Cytokines and fever. Front. Biosci. 9, 1433. https://doi.org/10.2741/1341.
Coomes, E.A., Haghbayan, H., 2020. Interleukin-6 in Covid-19: a systematic review and meta-analysis. Rev. Med. Virol. 30, 1–9. https://doi.org/10.1002/rmv.2141.
Cruz-Albarran, I.A., Rodríguez-Medina, D.A., Leija-Alva, G., Dominguez-Trejo, B., Osornio-Rios, R.A., Morales-Hernandez, L.A., 2020. Physiological stressor impact on peripheral facial temperature, Il-6 and mean arterial pressure, in young people. J. Therm. Biol. 91, 102616 https://doi.org/10.1016/j.jtherbio.2020.102616.
Dagdanpurev, S., Sun, G., Choimaa, L., Abe, S., Matsui, T., 2018. Clinical application of multiple vital signs-based infection screening system in a Mongolian hospital: optimization of facial temperature measurement by thermography at various ambient temperature conditions using linear regression analysis. In: Proc. Annu. Int. Conf. IEEE Eng. Med. Biol. Soc. EMBS, pp. 5313–5316. https://doi.org/10.1109/EMBC.2018.8513513, 2018-July.
Fawcett, T., 2006. An introduction to ROC analysis. Pattern Recogn. Lett. 27, 861–874. https://doi.org/10.1016/j.patrec.2005.10.010.
Fitriyah, H., Rachmadi, A., Setyawan, G.E., 2017. Automatic measurement of human body temperature on thermal image using knowledge-based criteria. J. Inf. Technol. Comput. Sci. 2 https://doi.org/10.25126/jitecs.20172235.
Ghassemi, P., Joshua Pfefer, T., Casamento, J.P., Simpson, R., Wang, Q., Pfefer, T.J., Casamento, J.P., Simpson, R., Wang, Q., 2018. Best practices for standardized performance testing of infrared thermographs intended for fever screening. PLoS One 13, e0203302. https://doi.org/10.1371/journal.pone.0203302.
Goeijenbier, M., van Kampen, J.J.A., Reusken, C.B.E.M., Koopmans, M.P.G., van Gorp, E. C.M., 2014. Ebola virus disease: a review on epidemiology, symptoms, treatment and pathogenesis. Neth. J. Med. 72, 442–448.
Gomolin, I.H., Aung, M.M., Wolf-Klein, G., Auerbach, C., 2005. Older is colder: temperature range and variation in older people. J. Am. Geriatr. Soc. 53, 2170–2172. https://doi.org/10.1111/j.1532-5415.2005.00500.x.
Gowen, B.B., Julander, J.G., London, N.R., Wong, M.H., Larson, D., Morrey, J.D., Li, D.Y., Bray, M., 2010. Assessing changes in vascular permeability in a hamster model of viral hemorrhagic fever. Virol. J. 7, 1–13. https://doi.org/10.1186/1743-422X-7-240.
Hay, A.D., Peters, T.J., Wilson, A., Fahey, T., 2004. The use of infrared thermometry for the detection of fever. Br. J. Gen. Pract. 54, 448–450.
Hesamian, M.H., Jia, W., He, X., Kennedy, P., 2019. Deep learning techniques for medical image segmentation: achievements and challenges. J. Digit. Imag. 32, 582–596. https://doi.org/10.1007/s10278-019-00227-x.
Hewlett, A.L., Kalil, A.C., Strum, R.A., Zeger, W.G., Smith, P.W., 2011. Evaluation of an infrared thermal detection system for fever recognition during the H1N1 influenza pandemic. Infect. Control Hosp. Epidemiol. 32, 504–506. https://doi.org/10.1086/659404.
Huang, C., Wang, Y., Li, X., Ren, L., Zhao, J., Hu, Y., Zhang, L., Fan, G., Xu, J., Gu, X., Cheng, Z., Yu, T., Xia, J., Wei, Y., Wu, W., Xie, X., Yin, W., Li, H., Liu, M., Xiao, Y., Gao, H., Guo, L., Xie, J., Wang, G., Jiang, R., Gao, Z., Jin, Q., Wang, J., Cao, B., 2020. Clinical features of patients infected with 2019 novel coronavirus in Wuhan, China. Lancet 395, 497–506. https://doi.org/10.1016/S0140-6736(20)30183-5.
International Electrotechnical Commission & International Organization for Standardization, 2017. IEC 80601-2-59:2017 Medical Electrical Equipment — Part 2-59: Particular Requirements for the Basic Safety and Essential Performance of Screening Thermographs for Human Febrile Temperature Screening.
International Organization for Standardization, 2017. ISO/TR 13154:2017 Medical Electrical Equipment - Deployment, Implementation and Operational Guidelines for Identifying Febrile Humans Using a Screening Thermograph.
Jessen, C., 1985. Thermal afferents in the control of body temperature. Pharmacol. Ther. 28, 107–134. https://doi.org/10.1016/0163-7258(85)90085-3.
Li, Q., Guan, X., Wu, P., Wang, X., Zhou, L., Tong, Y., Ren, R., Leung, K.S.M., Lau, E.H.Y., Wong, J.Y., Xing, X., Xiang, N., Wu, Y., Li, C., Chen, Q., Li, D., Liu, T., Zhao, J., Liu, M., Tu, W., Chen, C., Jin, L., Yang, R., Wang, Q., Zhou, S., Wang, R., Liu, H., Luo, Y., Liu, Y., Shao, G., Li, H., Tao, Z., Yang, Y., Deng, Z., Liu, B., Ma, Z., Zhang, Y., Shi, G., Lam, T.T.Y., Wu, J.T., Gao, G.F., Cowling, B.J., Yang, B., Leung, G.M., Feng, Z., 2020. Early transmission dynamics in Wuhan, China, of novel coronavirus-infected pneumonia. N. Engl. J. Med. 382, 1199–1207. https://doi.org/10.1056/NEJMoa2001316.
Liu, C.-C., Chang, R.-E., Chang, W.-C., 2004. Limitations of forehead infrared body temperature detection for fever screening for severe acute respiratory syndrome. Infect. Control Hosp. Epidemiol. 25, 1109–1111. https://doi.org/10.1086/502351.
Liu, T., Zhang, Jieying, Yang, Y., Zhang, L., Ma, H., Li, Z., Zhang, Jiaoyue, Cheng, J., Zhang, X., Wu, G., Yi, J., 2020. The potential role of IL-6 in monitoring coronavirus disease 2019. SSRN Electron. J. https://doi.org/10.2139/ssrn.3548761, 2019.
Martinez-Jimenez, M.A., Loza-Gonzalez, V.M., Kolosovas-Machuca, E.S., Yanes-Lane, M. E., Ramirez-GarciaLuna, A.S., Ramirez-GarciaLuna, J.L., 2021. Diagnostic accuracy of infrared thermal imaging for detecting COVID-19 infection in minimally symptomatic patients. Eur. J. Clin. Invest. 51 https://doi.org/10.1111/eci.13474.
McGonagle, D., Sharif, K., O'Regan, A., Bridgewood, C., 2020. The role of cytokines including interleukin-6 in COVID-19 induced pneumonia and macrophage activation syndrome-like disease. Autoimmun. Rev. 102537 https://doi.org/10.1016/j.autrev.2020.102537.
Mercer, J.B., Ring, E.F.J., 2003. Fever screening and infrared thermal imaging: concerns and guidelines. Thermol. Int. 19, 67–69.
Michelen, M., Jones, N., Stavropoulou, C., 2020. In patients of COVID-19, what are the symptoms and clinical features of mild and moderate cases? [WWW Document]. Oxford COVID-19 Evid. Serv. Team Cent. Evidence-Based Med. URL. https://www.cebm.net/covid-19/in-patients-of-covid-19-what-are-the-symptoms-and-clinical-features-of-mild-and-moderate-case/. (Accessed 4 August 2020).
Mouchtouri, V.A., Christoforidou, E.P., Heiden, M. der, Lemos, C.M., Fanos, M., Rexroth, U., Grote, U., Belfroid, E., Swaan, C., Hadjichristodoulou, C., 2019. Exit and entry screening practices for infectious diseases among travelers at points of entry: looking for evidence on public health impact. Int. J. Environ. Res. Publ. Health 16, 4638. https://doi.org/10.3390/ijerph16234638.
Ng, D.K., Chan, C.-H., Lee, R.S., Leung, L.C., 2005a. Non-contact infrared thermometry temperature measurement for screening fever in children. Ann. Trop. Paediatr. 25, 267–275. https://doi.org/10.1179/146532805X72412.
Ng, E.Y.K., 2012. Thermal imager as fever identification tool for infectious diseases outbreak. In: Medical Infrared Imaging. CRC Press, pp. 1–20. https://doi.org/10.1201/b12938-25.
Ng, E.Y.K., 2004. Is thermal scanner losing its bite in mass screening of fever due to SARS? Med. Phys. 32, 93–97. https://doi.org/10.1118/1.1819532.
Ng, E.Y.K., Acharya, R., 2009. Remote-sensing infrared thermography. IEEE Eng. Med. Biol. Mag. 28, 76–83. https://doi.org/10.1109/MEMB.2008.931018.
Ng, E.Y.K., Chong, C., 2006. ANN-based mapping of febrile subjects in mass thermogram screening: facts and myths. J. Med. Eng. Technol. 30, 330–337. https://doi.org/10.1080/03091900500225136.
Ng, E.Y.K., Chong, C., Kaw, G.J.L., 2005b. Classification oh human facial and aural temperature using neural networks and IR fever scanner: a responsible second look. J. Mech. Med. Biol. 165–190. https://doi.org/10.1142/S0219519405001370, 05.
n.d Ng, E.Y.K., Kaw, G.J.L., 2006. IR imagers as fever monitoring devices: physics, physiology, and clinical accuracy. In: Bronzino, J.D. (Ed.), Medical Devices and Systems. Taylor & Francis, Boca Raton.
Ng, E.Y.K., Kawb, G.J.L., Chang, W.M., 2004. Analysis of IR thermal imager for mass blind fever screening. Microvasc. Res. 68, 104–109. https://doi.org/10.1016/j.mvr.2004.05.003.
Ng, E.Y.K., Kee, E.C., 2008. Fever mass screeing tool for infectious diseases outbrake: integrated artificial intelligence with bio-statistical approach in thermogram analysis. In: Diakides, N.A., Bronzino, J.D. (Eds.), Medical Infrared Imaging. CRC Press, Boca Raton.
Ng, E.Y.K., Muljo, W., Wong, B.S., 2006. Study of facial skin and aural temperature. IEEE Eng. Med. Biol. Mag. 25, 68–74. https://doi.org/10.1109/MEMB.2006.1636353.
Nguyen, A.V., Cohen, N.J., Lipman, H., Brown, C.M., Molinari, N.-A., Jackson, W.L., Kirking, H., Szymanowski, P., Wilson, T.W., Salhi, B.A., Roberts, R.R., Stryker, D.W., Fishbein, D.B., 2010. Comparison of 3 infrared thermal detection systems and self-report for mass fever screening. Emerg. Infect. Dis. 16, 1710–1717. https://doi.org/10.3201/eid1611.100703.
Nishiura, H., Kamiya, K., 2011. Fever screening during the influenza (H1N1-2009) pandemic at narita international airport, Japan. BMC Infect. Dis. 11, 111. https://doi.org/10.1186/1471-2334-11-111.
Omori, R., Matsuyama, R., Nakata, Y., 2020. The age distribution of mortality from novel coronavirus disease (COVID-19) suggests no large difference of susceptibility by age. Sci. Rep. 10, 1–9. https://doi.org/10.1038/s41598-020-73777-8.
Pascoe, D.D., 2010. Comparison of measuring sites for the assessment of body temperature: final amendment. Thermol. Int. 20, 36–38.
Quilty, B.J., Clifford, S., Flasche, S., Eggo, R.M., 2020. Effectiveness of airport screening at detecting travellers infected with novel coronavirus (2019-nCoV). Euro Surveill. 25 https://doi.org/10.2807/1560-7917.ES.2020.25.5.2000080.
Ring, E.F.J., Jung, A., Kalicki, B., Zuber, J., Rustecka, A., Vardasca, R., 2013. New standards for fever screening with thermal imaging systemss. J. Mech. Med. Biol. 13 https://doi.org/10.1142/S0219519413500450.
Ring, F.J., Ng, E.Y.K., 2012. Infrared thermal imaging standards for human fever detection. In: Medical Infrared Imaging: Principles and Practices. https://doi.org/10.1201/b12938, 22-1-22–6.
Rodríguez-Medina, D.A., 2018. The infrared thermal image and citokine il-6 in the affective diagnosis of patients with non-communicable chronic diseases. Biomed. J. Sci. Tech. Res. 4 https://doi.org/10.26717/bjstr.2018.04.0001102.
Saper, C.B., 1998. Neurobiological basis of fever. Ann. N. Y. Acad. Sci. 856, 90–94. https://doi.org/10.1111/j.1749-6632.1998.tb08317.x.
Selent, M.U., Molinari, N.M., Baxter, A., Nguyen, A.V., Siegelson, H., Brown, C.M., Plummer, A., Higgins, A., Podolsky, S., Spandorfer, P., Cohen, N.J., Fishbein, D.B., 2013. Mass screening for fever in children. Pediatr. Emerg. Care 29, 305–313. https://doi.org/10.1097/PEC.0b013e3182854465.
Shi, H., Han, X., Jiang, N., Cao, Y., Alwalid, O., Gu, J., Fan, Y., Zheng, C., 2020. Radiological findings from 81 patients with COVID-19 pneumonia in Wuhan, China: a descriptive study. Lancet Infect. Dis. 20, 425–434. https://doi.org/10.1016/S1473-3099(20)30086-4.
Sun, G., Matsui, T., Kirimoto, T., Yao, Y., Abe, S., 2017. Applications of infrared thermography for noncontact and noninvasive mass screening of febrile international travelers at airport quarantine stations. In: Application of Infrared to Biomedical Sciences. Springer, pp. 347–358. https://doi.org/10.1007/978-981-10-3147-2_19.
Tan, C.L., Knight, Z.A., 2018. Regulation of body temperature by the nervous system. Neuron 98, 31–48. https://doi.org/10.1016/j.neuron.2018.02.022.
Taylor, S., Wakem, M., Dijkman, G., Alsarraj, M., Nguyen, M., 2010. A practical approach to RT-qPCR—publishing data that conform to the MIQE guidelines. Methods 50, S1–S5. https://doi.org/10.1016/j.ymeth.2010.01.005.
Teran, C.G., Torrez-Llanos, J., Teran-Miranda, T.E., Balderrama, C., Shah, N.S., Villarroel, P., 2012. Clinical accuracy of a non-contact infrared skin thermometer in paediatric practice. Child Care Health Dev. 38, 471–476. https://doi.org/10.1111/j.1365-2214.2011.01264.x.
U.S. Department of Health and Human Services, Food and Drug Administration, Center for Devices and Radiological Heah (CDRH), Office of Product Evaluation and Quality (OPEQ), 2020. Enforcement Policy for Telethermographic Systems during the

Coronavirus Disease 2019 (COVID-19) Public Health Emergency: Guidance for Industry and Food and Drug Administration Staff 2019.

Valueva, M.V., Nagornov, N.N., Lyakhov, P.A., Valuev, G.V., Chervyakov, N.I., 2020. Application of the residue number system to reduce hardware costs of the convolutional neural network implementation. Math. Comput. Simulat. 177, 232–243. https://doi.org/10.1016/j.matcom.2020.04.031.

van Belle, G., 2008. Statistical rules of thumb, second ed. In: Wiley Series in Probability and Statistics. John Wiley & Sons, Inc., Hoboken, NJ, USA https://doi.org/10.1002/9780470377963.

Vardasca, R., Magalhaes, C., Marques, D., Moreira, J., Frade, R., Seixas, A., Mendes, J., Ring, E.F.J., Ring, F., 2019. Bilateral assessment of body core temperature through axillar, tympanic and inner canthi thermometers in a young population. Physiol. Meas. 40, 094001 https://doi.org/10.1088/1361-6579/ab2af6.

Venkatesan, P., 2020. The changing demographics of COVID-19. Lancet Respir. Med. 8, e95 https://doi.org/10.1016/s2213-2600(20)30461-6.

Wedderburn, L., Peckham, H., De Gruijter, N., Raine, C., Radziszewska, A., Ciurtin, C., Rosser, E., Deakin, C., Webb, K., 2020. Male sex identified by global COVIS-19 meta-analysis as a risk factor for death and ITU admission. Nat. Commun. 1–10. https://doi.org/10.21203/rs.3.rs-23651/v2.

Yang, X., Yu, Y., Xu, J., Shu, H., Xia, J., Liu, H., Wu, Y., Zhang, L., Yu, Z., Fang, M., Yu, T., Wang, Y., Pan, S., Zou, X., Yuan, S., Shang, Y., 2020. Clinical course and outcomes of critically ill patients with SARS-CoV-2 pneumonia in Wuhan, China: a single-centered, retrospective, observational study. Lancet Respir. Med. 8, 475–481. https://doi.org/10.1016/S2213-2600(20)30079-5.

Zhou, Y., Ghassemi, P., Chen, M., Mcbride, D., Casamento, J.P., Pfefer, T.J., Wang, Q., 2020. Clinical evaluation of fever-screening thermography: impact of consensus guidelines and facial measurement location. J. Biomed. Opt. 25, 1–21. https://doi.org/10.1117/1.jbo.25.9.097002.